NANO LETTERS

pubs.acs.org/NanoLett

Letter

Probing Correlation of Optical Emission and Defect Sites in Hexagonal Boron Nitride by High-Resolution STEM-EELS

Sakal Singla,[#] Pragya Joshi,[#] Gabriel I. López-Morales,[*] Suman Sarkar, Suman Sarkar, Johannes Flick, and Biswanath Chakraborty[*]

Cite This: *Nano Lett.* 2024, 24, 9212−9220

Read Online

ACCESS | Metrics & More | Article Recommendations | Supporting Information

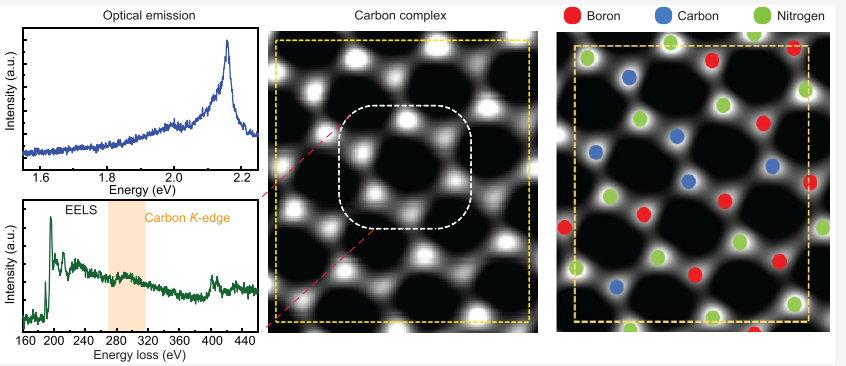

ABSTRACT: Optically bright emitters in hexagonal boron nitride (hBN) often acting as a source of a single-photon are mostly attributed to point-defect centers, featuring localized intra-bandgap electronic states. Although vacancies, anti-sites, and impurities have been proposed as candidates, the exact physical and chemical nature of most hBN single-photon emitters (SPEs) within the visible region are still up for debate. Combining site-specific high-angle annular dark-field imaging (HAADF) with electron energy loss spectroscopy (EELS), we resolve and identify a few carbon substitutions among neighboring hBN hexagons, all within the same sample region, from which typical defect emission is observed. Our experimental results are further supported by first-principles calculations, through which the stability and possible optical transitions of the proposed carbon-defect complex are assessed. The presented correlation between optical emission and defects provides valuable information toward the controlled creation of emitters in hBN, highlighting carbon complexes as another probable cause of its visible SPEs.

KEYWORDS: *hBN, defects, carbon, DFT, STEM-EELS*

Hexagonal boron nitride (hBN) is a wide bandgap material, making it a suitable candidate to host various sub-bandgap defect states. Extensive research has shown that these defect states act like single-photon emitters (SPEs), capable of emitting over a broad spectral range covering UV to NIR.[1−5] At the same time hBN emitters exhibit interesting properties, such as relative high brightness,[6,7] stable room-temperature operation,[8,9] and potential for efficient integration with photonic platforms.[10,11] These defect states in hBN are often created using different methods[12−16] but can also be inherently present due to certain growth techniques.[17−20] The optical properties of emissions in hBN have been extensively studied. For instance, Grosso et al. observed 579 nm (2.145 eV) emission created by FIB and attributed it to the nitrogen anti-site defect.[15] Kumar et al. reported emitters with a 575 nm zero-phonon line (ZPL) and (through first-principles simulations) suggested a carbon complex and a carbon-vacancy defect as probable causes of the emission.[21,22] Along with experiments, first-principles modeling has also played an important role in identifying defect-related emitters in solids.[23−25] From this perspective, point defects like vacancies, impurity substitutions/interstitials, and combinations of these, are among the candidates behind the sub-bandgap emission in hBN,[26−29] although dangling bonds and more complicated defect complexes have been recently proposed.[30−35]

Overall, there seems to be a large pool of microscopic candidates for the observed emission in hBN. This is largely driven by the disparity in observed optical properties (e.g., blinking and possibly large Stark-shifts), sample preparation/treatments, and the lack of correlation between emission sites and their atomic structures. Recent work along these directions

Received: March 27, 2024
Revised: June 12, 2024
Accepted: June 12, 2024
Published: June 18, 2024

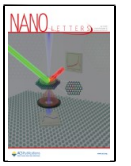

https://doi.org/10.1021/acs.nanolett.4c01477
Nano Lett. 2024, 24, 9212−9220

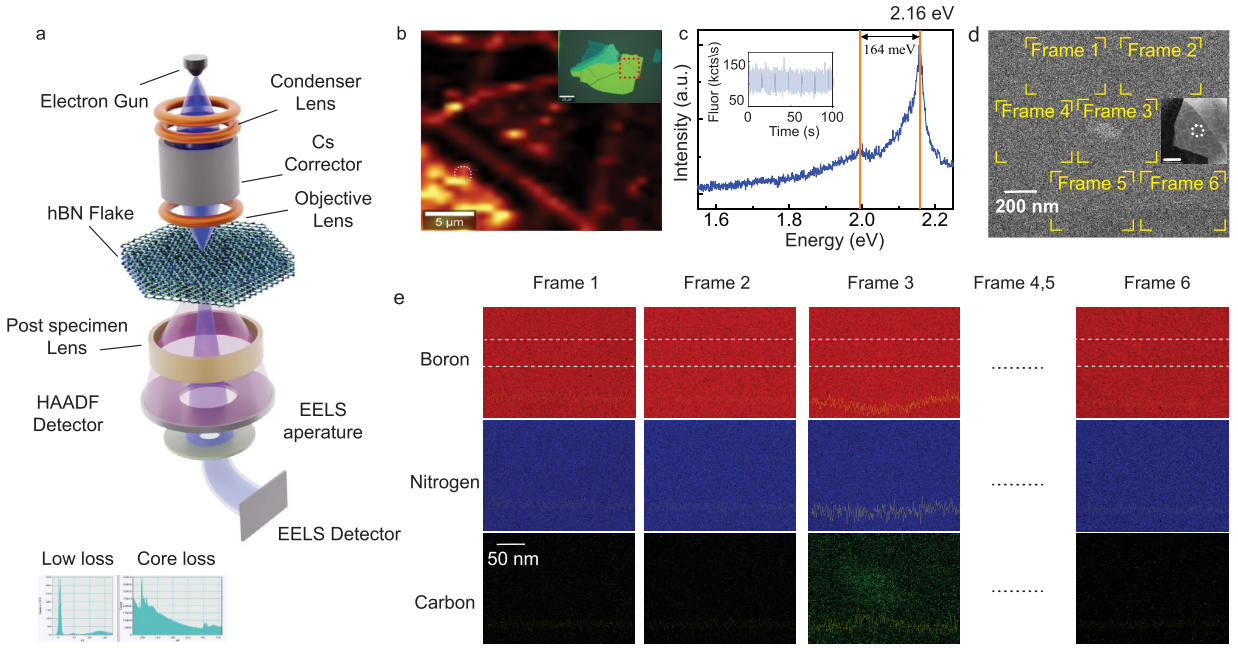

Figure 1. Spotting the emissive region in the TEM. (a) Schematic of electron energy-loss spectroscopy incorporated in a scanning transmission electron microscope. (b) Confocal PL image of hBN flake with multiple emission sites. The inset displays the optical image of the same flake where red square box indicates the area of PL scanning. (c) Photoluminescence (PL) spectrum obtained from the region encircled in (b). The central wavelengths of the ZPL and its PSB are identified, with a relative shift of ∼ 164 meV (the TO-phonon energy in hBN[36]). (d) Low-resolution HAADF image of the emission region shown marked by the white circle in (b). The different frames are marked. The inset shows the low-magnification image of the flake in the TEM. Dotted circles represent the same region divided into frames. The inset scale bar is 5 μm. (e) EELS elemental map of boron, carbon, and nitrogen K edges for different frames. For frames "4" and "5", see Section S4 of the Supporting Information. The yellow line in each frame represents the EELS intensity profile obtained from integrating over the white dotted area. The intensity graph as a function of distance is also shown in Section S4.

includes the correlation between optical emission to local strain in hBN nanoflakes via cathodoluminescence (CL) and nanobeam electron diffraction (NBD),[2] as well as the study of carbon substitutions as cause of photobleaching in hBN emitters through dark-field imaging.[37]

Thus far, defect studies in hBN have mostly involved high-resolution dark-field imaging,[37−39] wherein the identification depends on site-specific image contrast. Relying on some sort of elemental-specific spectroscopic signal could result in a more accurate assessment of the local chemical environment near the emission sites. For instance, core-level spectroscopy techniques where the inner-shell electrons are excited, provide information about the underlying electronic structure, composition, and bonding properties.[40,41] Among these, electron energy-loss spectroscopy (EELS) can be particularly useful for atomic-scale elemental analysis.[42−44] In scanning transmission electron microscopy EELS (STEM-EELS), a focused electron beam is directed toward the sample (Figure 1a) and scanned over each atom. As the high-energy electrons interact with it, they lose energy mostly through inelastic scattering and ionization processes. The scattered electrons are collected and directed into an energy analyzer, based on their energy losses. The spectroscopic analysis of such energy losses in the electron beam as it travels through the sample is what is known as EELS. The amount of energy lost depends on the nature of the interaction and the composition of the sample, resulting in elemental-specific signatures. As an additional advantage, atomic resolution can be obtained when EELS is coupled with high-angle annular dark-field (HAADF) based STEM imaging, i.e., individual atoms are resolved in STEM mode, followed by EELS acquisition, to perform atom-by-atom elemental identification.

The sample was prepared by dry-exfoliating hBN onto a Si/SiO_2 substrate. After optical inspection under the microscope, a visibly thick flake was chosen. The height determined by atomic force microscopy (AFM) was ∼60 nm (height profile in Figure S1). Similar thicknesses are reported to host stable emitters in hBN.[15,45] We bombarded random locations of the flake in the field emission scanning electron microscope (FESEM) to create emitters.[46] The electron beam acceleration was kept at 20 kV, and a probe current of 60 pA was used. Subsequently, the substrate was annealed at 850 °C in an argon atmosphere for 2 h under an optimized flow rate of 1 bubble per second (corresponds to ∼ 20 sccm). Despite formation of defect sites being a stochastic process,[14,47] their precise location (down to the diffraction limit) can be determined by scanning the flake for observable defect-mediated emission. A confocal photoluminescence (PL) scan of the flake (Figure 1b) shows a few such localized bright emission spots. The scan was performed using sub-bandgap laser excitation of 2.33 eV with an incident power of 100 μW. The PL spectrum in Figure 1c from the white dashed circle (in Figure 1b) is characterized by two distinct features: a sharp ZPL centered around 2.160 eV (574 nm) and a relatively broad phonon sideband (PSB) at 1.996 eV (621 nm). The emission was observed to be stable, as is evident from the time trace curve in the inset. Similar spectral features with identical energy separation between ZPL and PSB have been reported in previous studies on hBN quantum emitters[3,18,48] and is attributed to optically active point defects. The emission

https://doi.org/10.1021/acs.nanolett.4c01477
Nano Lett. 2024, 24, 9212−9220

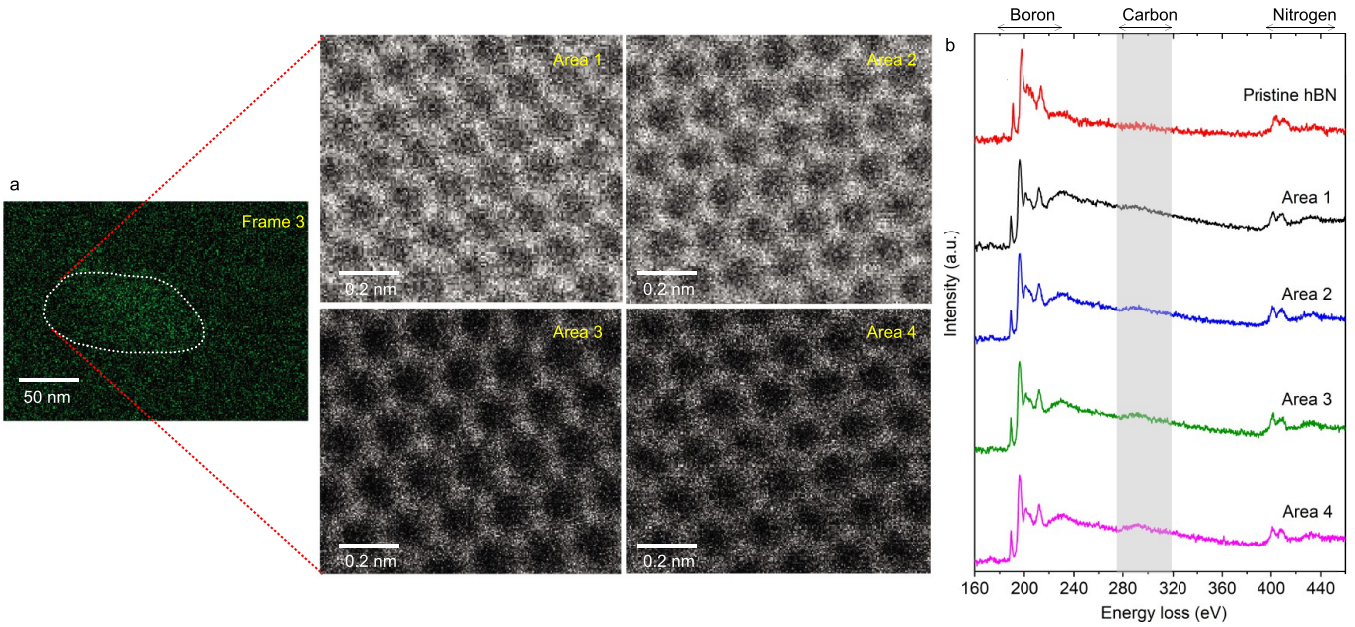

Figure 2. Atomically resolved hBN lattice indicating the presence of carbon. (a) High-resolution HAADF-STEM micrographs taken from the carbon-dense region (shown by a white dotted area) in "Frame 3". (b) EELS spectra acquired from areas "1" to "4". The EELS spectrum from pristine hBN is also shown for reference.

spectrum from other bright spots does not show such prominent PL peaks (Supplementary, Section S2).

In order to correlate the optical spectra with potential underlying defects, we carried out structural investigation of the emissive region at the atomic level in an aberration corrected TEM (JEOL NEO ARM 200F) instrument equipped with a cold field emission gun. The flake was imaged at an accelerating voltage of 200 kV. Using low-resolution imaging, the optically active region of the flake was first located. For this purpose, we aligned the flake edges (Supplementary, Section S3) with respect to the corresponding optical image (dotted rectangle in Figure 1b inset). Subsequently, the selected area (dashed white circle in inset of Figure 1d) was spectrally mapped using EELS. To minimize the effect of sample drifting, we performed EELS scans over smaller frames (~250 × 200 nm^2). The elemental map in Figure 1e depicts pixel intensities of parent boron (red) and nitrogen (in blue). The line intensity profile across the frame denotes the pixel intensity values integrated over the white dashed area. Notably, in "Frame 3" the presence of carbon is revealed by a streak of closely spaced green dots mainly confined within a small patch near the center (see the dotted region in Figure 2a). The carbon intensity shows a hump over the patch. The intensity profile in each frame is shifted for clarity. It is to be noted that the increase in carbon hump is marked by a slight dip in boron while for nitrogen it remains almost flat. This indicates that boron is preferentially substituted[49] by carbon. With the confirmation of carbon being present in hBN, we further monitored the same region in high-resolution mode to study the underlying microscopic details. This would help us to obtain a clear picture of the atomic arrangement of defect sites from where we observed optical emission.

Figure 2a shows several high-resolution HAADF-STEM images captured from various microscopic regions ("Area 1", "Area 2", etc.) that make up the carbon patch (see the dotted region in Figure 2a) in "Frame 3". Details of imaging parameters are given in the Methods section. This was followed by a swift EELS scan performed over the same areas using a pixel size of 0.028 nm and dwell time 0.02 s to ensure optimal acquisition time. The corresponding EELS spectra integrated over area is displayed in Figure 2b. The highlight of the spectra (except for the top one) is the appearance of the characteristic carbon K-edge signature ~285 eV, in addition to boron and nitrogen signals occurring around 200 and 400 eV, respectively. In order to rule out the possibility of carbon incorporation in TEM, we recorded the EELS spectrum from pristine hBN (top spectrum in Figure 2b) where the signal at 280 eV is absent. The pristine hBN part is discussed in Section S5 of the Supplementary. Other high-resolution images along with their corresponding EELS spectra are available in the Supporting Information, Section S9. For the remainder of the paper, we concentrate on the atomic configuration in "Area 4" since it presents the most intense carbon peak.

The line intensity profile of the HAADF image is known to be proportional to the atomic number of elements present in the structure.[38] Since nitrogen has a higher atomic number than boron, it will appear brighter. Carbon by extension would have an intensity that lies between that of nitrogen and boron. Using fast Fourier transformation (FFT) to get a high signal-to-noise ratio, we were able to achieve a sub-angstrom spatial resolution to distinguish individual atoms in the hBN lattice. This is evident in Figure 3a where the intensity variation for adjacent atoms was also observed. The intensity profile along line L4 in Figure 3b shows three distinct crests: nitrogen (highest one), boron (lowest), and carbon (intermediate). Line scans along L1 and L3 also help to spot nitrogen, boron, and carbon. Based on these intensity profiles, we identify the atoms corresponding to different sites for the hexagon R1 (shown by white boundary). To further substantiate our atomic markings, Figure 3c shows EELS spectra from individual hexagons in the region. The carbon K-edge around 285 eV is present in the spectrum from hexagon marked R1. For reference, the EELS spectrum from the adjacent region (P)

https://doi.org/10.1021/acs.nanolett.4c01477
Nano Lett. 2024, 24, 9212−9220

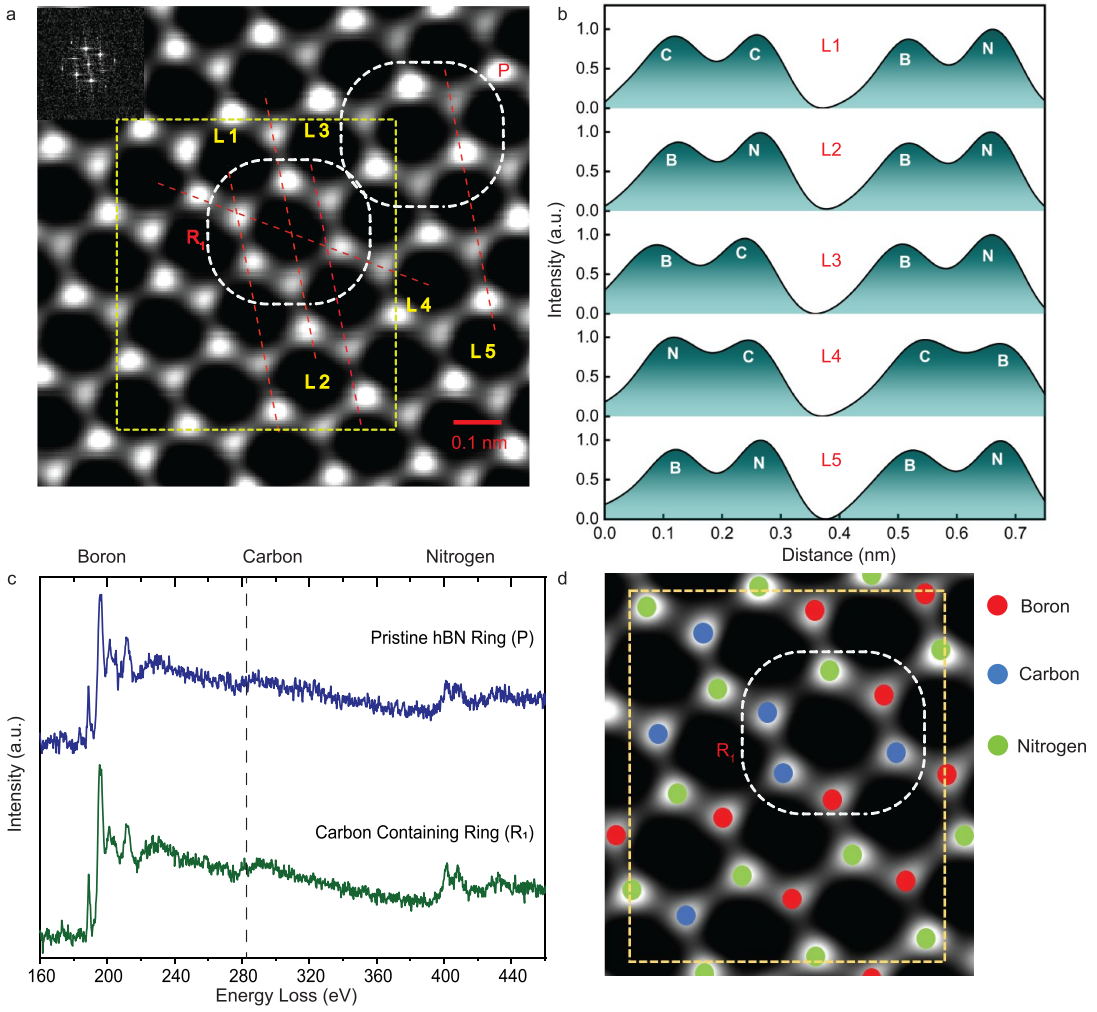

Figure 3. Arrangement of carbon in hBN. (a) Inverse FFT image of "Area 4" showing significant intensity variation across different atomic sites. The dashed rectangular region is considered for theoretical modeling. Inset: corresponding fast Fourier frequency pattern in the reciprocal space of area 4. (b) Intensity profiles along different lines marked L1, L2, L3, L4, and L5. Region R1 has carbon, while region P is pristine. The intensity is normalized with respect to the nitrogen atom intensity. (c) EELS spectra recorded from P (top) and R1 (bottom). The carbon K-edge around 285 eV is indicated by a dashed line. (d) Magnified version of the dashed rectangular region in (a) with atoms marked.

is also depicted. It is characterized by boron and nitrogen with little or no evidence of carbon. The remaining HAADF intensity profile and EELS spectra from within the region are shown in Section S7 of the Supporting Information. Thus, using the dual identification protocol comprising HAADF-STEM imaging and scanning EELS, we can label each atom in "Area 4". Figure 3d depicts such a case, where atoms have been labeled based on the obtained HAADF-STEM and EELS data. We can see that carbon is replacing both nitrogen and boron in some of the atomic sites (for a complete picture, see Section S6 of the Supporting Information). Overall, the experimental results suggest that this carbon-complex structure could be responsible for the optical emission obtained from this sample region. We investigate this further through first-principles calculations, as discussed below in the next section.

We made use of density functional theory (DFT) to support the experimental identification mechanisms employed in this work. We start by considering a slightly simplified version (Figure 4a) of the full carbon-complex defect structure proposed from experiments (see Supplementary, Section S6). In this way, we attempt to minimize the complexity of the defect structure within the finite-size simulation cell, while aiming to get an idea of the hybridization effects and interdefect interactions among the neighboring carbon substitutions. These are some of the key aspects of the results described herein, compared to previous recent work on carbon defects in hBN.[31−34,51] Altogether, our defect complex (dotted square in Figure 4a) consists of a carbon dimer (C_BC_N) and a set of four carbon substitutions (three C_B and one C_N), three of which are "nearest-neighbor" to the dimer, in line with (Figure 3d) from experiments.

Figure 4b presents the calculated charge-state transition levels for the defect complex in Figure 4a. From these results, we see that this defect complex could exist in five different charge states depending on the "local Fermi level". It should be noted, however, that typical hBN samples have Fermi levels above the midgap.[52] Assuming the sample studied herein is typical, we focus on the +1, 0, and −1 charge states, as they are the most likely to form. In Figure 4c we plot the Kohn−Sham (KS) eigenvalues of the carbon complex in the relevant charge states (with the +2 case added as a reference to make the trend across the charge states clearer). These defect complexes feature a number of defect states within the bandgap of hBN, which arise from the combination of individual substitutions

https://doi.org/10.1021/acs.nanolett.4c01477
Nano Lett. 2024, 24, 9212−9220

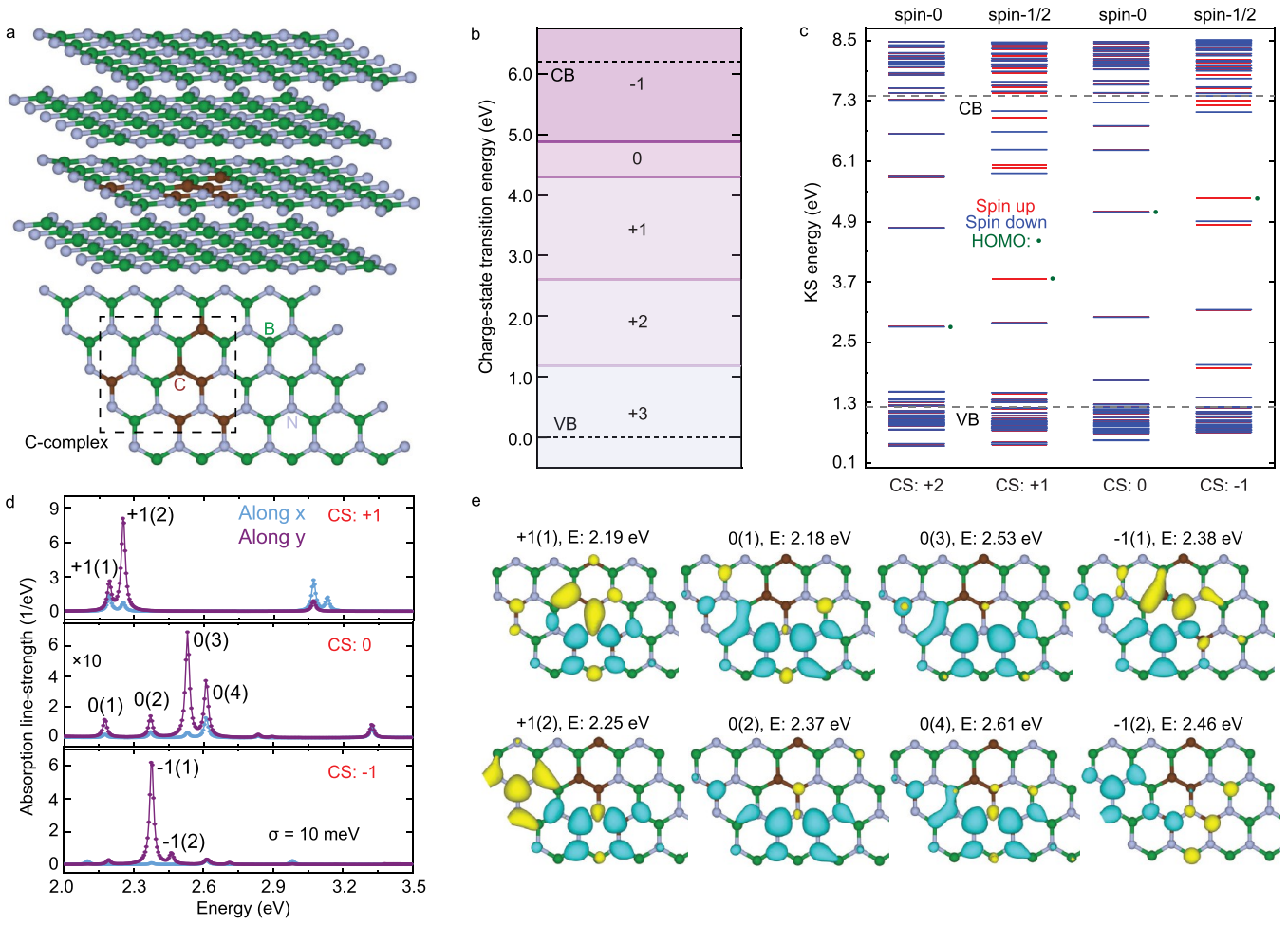

Figure 4. First-principles modeling of experimental defect structure. (a) Atomic structure of the carbon defect complex in bulk hBN used in our calculations, formed by six carbon atoms substituting neighboring boron and nitrogen sites (dashed square in lower panel). (b) Thermodynamic charge-state stability. (c) Energy levels for some of the defect charge states from (b). (d) Absorptive transition dipole moments (TDMs) between frontier (10 occupied/unoccupied) defect states. Only the transitions with energies falling within the spectral region of interest are shown. (e) Transition densities for the peaks outlined in (d). All isosurfaces are set to 1×10^{-6}.

considered within the complex, with some degree of mixing/hybridization due to their spatial proximity.

From the energy levels in Figure 4c we see that, in principle, intra-bandgap electronic transitions are possible for the three defect charge states of this carbon complex, either from corresponding highest-occupied molecular orbitals (HOMO) or from lowest-energy occupied defect states lying within the bandgap. In order to pinpoint possible similarities between the optical transitions of this complex and the optical features typically observed in defect-related quantum emitters in hBN (e.g., Figure 1c), we calculate the transition-dipole moment (TDM) matrix elements. This would be analogous to calculating the "dielectric response" at the defect site (see Section S10 of the Supporting Information for further details). In doing so, we consider transitions between the highest 10 occupied and lowest 10 unoccupied states of the carbon complex to include potential shallow bulk-to-defect or mixed transitions.

The obtained results are summarized in Figure 4d. In all three charge states, we find plausible transitions that lie close to (or below) the excitation energy relevant for experiments (~2.33 eV). With this, given the relatively small Franck–Condon shifts and Huang–Rhys factors for tentative carbon-based and intrinsic point defects studied in hBN,[28,31,34,53] we think it is possible that such carbon complexes have optical features similar to those observed in experiment, in particular, reminiscent of those corresponding to isolated (or paired) substitutions. Interestingly, there seems to be a relative suppression (~10-fold) of the optical activity of this complex when in its neutral charge state (second panel of Figure 4d). Given the relative proximity of the charge-state transition levels, this could translate into optical "blinking" behavior under constant illumination. Lastly, a good number of apparent optical transitions within the studied excitation region have decently high degrees of linear polarization (blue versus purple lines). This can be further seen from the transition densities in Figure 4e, plotted for some of the transitions in Figure 4d (marked with "charge state (transition number)". This is another key feature typical of SPE from hBN, and could also hint at possible disentangled contributions from the individual components of the defect complex studied herein (e.g., single-carbon substitution). For instance, most of the transition densities show a lack of contribution from carbon members within the full defect complex. These observations tie well with the previous notion of such complexes as "weakly interacting single-carbon defects" in hBN. Overall, given the results outlined herein, we suggest carbon complexes like the one studied herein could be partly responsible for the observed

https://doi.org/10.1021/acs.nanolett.4c01477
Nano Lett. 2024, 24, 9212−9220

quantum emission from point defects in hBN. A comparison of our results to the existing reports in presented in Table 1.

Table 1. Comprehensive Summary of Our Results Compared against Results from Recent Relevant Studies on Carbon Defects in hBN[a]

Reference	Emission (eV)	Methodology	Defect/complex
This work	~2.16	HAADF; STEM-EELS	Carbon complex (obs)
Kumar et al.[21,22]	~2.15	DFT	C_BC_N C_BC_N (prop)
Zhong et al.[48]	~2.24	DFT	C_B-C_N DAP (prop)
Li et al.[37]	~1.98	STEM-ADF	Vac/C-subs (obs)
Mendelson et al.[18]	~2.12; 1.95	DFT; PL spectroscopy	V_BC_N (prop)
Tan et al.[50]	~2.18	DFT	$H_N^{(F)}-C_N^{(H)}$ DAP (prop)

[a]Notation: "obs" stands for observed, "prop" for proposed, "Vac" for vacancy, and "C-subs" for carbon substitutions.

In summary, we have established a direct experimental correlation between visible emission from point defects in hBN and the underlying atomic structure. Using high-resolution STEM-EELS, we propose a carbon complex to be responsible for the 2.16 eV emission in hBN. Thanks to the elemental-specific signatures obtained from EELS and HAADF image contrast, we observe the exact atomic configuration of the defect complex. The proposed defect configuration responsible for the 2.16 eV emission was further studied via first-principles calculations using DFT. Overall, the thermodynamic charge-state transitions, electronic structures, and possible optical features obtained from DFT support the carbon complex derived from experiments as a possible defect structure responsible for the observed optical emission. Our findings suggest an interesting alternative among the carbon-related defects behind hBN SPEs, in line with prior work but somewhat unexplored. Lastly, the experimental techniques explored in this work provide an interesting approach toward on-site identification of defect emission in solid-state materials, which could enhance creation and control of quantum emitters in these platforms.

METHODS

Sample Preparation. Bulk hBN crystal used for exfoliation was purchased from 2D semiconductors. Flakes were exfoliated using Scotch tape on a Si substrate with a 285 nm SiO_2 layer. The substrate was cleaned in acetone and isopropyl alcohol prior to exfoliation. For electron irradiation, the SEM chamber was evacuated to a pressure of 5×10^{-4}. Different areas of the flakes with a frame area of 1800×2400 nm^2 were irradiated for 20 s each. The sample was subsequently annealed in argon atmosphere at 850 °C for 2 h under continuous argon flow. The flow rate was adjusted to be at ~20 sccm.

Optical Measurements. All our optical measurements were done at room temperature in a customized WITEC Alpha 300 confocal microscope. A 532 nm continuous-wave (CW) laser was used for excitation and focused onto the sample using an Olympus 100× objective with a NA of 0.95. A 550 nm cut-on dichroic was used to suppress the back reflected laser from the light collected through the objective. The collected signal was fiber-coupled to a spectrometer (Princeton HRS 500) equipped with an Andor CCD camera. All spectra were acquired for 10 s using a 600 lines/mm optical grating.

STEM-EELS Measurements. HAADF-STEM images and EELS spectra were acquired using a JEOL NEO ARM 200F (equipped with Cs corrector and a postcolumn Gatan EELS spectrometer). The system has dedicated ultrahigh-vacuum STEM, combined with cold field-emission guns operating at 200 kV. HAADF-STEM imaging was recorded with the pixel size 0.0066 nm and dwell time 15 μs with the probe current of 16−18 pA. Also, HAADF inner and outer collection angles were set to 68 and 280 mrad, respectively. Using low-resolution STEM imaging, we found the location of the emitter by aligning the optical image of the flake. At the same time, elemental EELS mapping was carried on the same location (see Figure 1). Second, EELS spectra and spectral images of subnanometer areas (1.192×0.894 nm^2, with 40×30 pixels) covering a few atoms were recorded with the Gatan EELS spectrometer. An EELS spectral mapping with zero-loss has been captured with dispersion of 0.24 eV/ch (perfectly covering boron, carbon and nitrogen k edge signals), probe convergence angle of 28 mrad and collection angle of 12.5 mrad. Such dispersion really helps in aligning the boron and nitrogen k edge signals. Furthermore, to minimize the spatial drifting of the sample at the atomic resolution, we optimize the spectral image that has been acquired with a pixel size of 0.028 nm and a pixel time of 0.05 s. The total acquisition time for STEM-EELS experiments performed in this work amounted to ~ 2 min.

First-Principles Calculations. All DFT calculations have been performed using the Vienna *ab-initio* simulation package (VASP) code.[54] In VASP, the projector-augmented-wave (PAW) method is employed to treat core electrons in the form of atomic pseudopotentials.[55] The remaining valence electrons are treated explicitly, in our particular case using the Heyd−Scuseria−Ernzerhof (HSE) functional to approximate exchange-correlation interactions, with the exact-exchange mixing parameter $\alpha = 0.4$.[56,57] We use the scheme of Grimme to treat van der Waals interactions, which are key in simulating bulk hBN within DFT.[58−60] The valence electrons are expanded in the plane-wave basis using a kinetic-energy cutoff of 500 eV. To ensure atomic positions and wave functions are sufficiently converged, the optimizations run until forces and energy changes are below 10^{-3} and 10^{-6}, respectively. This global choice of simulation parameters is mostly based on previous work,[31,33,51] where they have provided reasonable treatment for the optoelectronic properties of carbon-related point defects in hBN. Further details regarding the defect structure and other parameters are included in Section S 10 of the Supporting Information.

ASSOCIATED CONTENT

Supporting Information

The Supporting Information is available free of charge at https://pubs.acs.org/doi/10.1021/acs.nanolett.4c01477.

Height-profile analysis of Sample 1 (Section S1), PL analysis of Sample 1 (Section S2), identifying emission site in TEM (Section S3), EELS elemental mapping of frames 4 and 5 (Section S4), HAADF-STEM micrographs and EELS of pristine hBN (Section S5), complete atomic identification within "Area 4" based on HAADF intensity (Section S6), elemental identi-

https://doi.org/10.1021/acs.nanolett.4c01477
Nano Lett. 2024, 24, 9212−9220

fication of pristine ring "P" (Section S7), EELS spectrum of rings "R2", "R3", and "R4" (Section S8), HAADF-STEM micrograph and EELS spectrum of areas "5−12" and their corresponding EELS spectra (Section S9), first-principles simulations (Section S10), "Sample 2" - EELS analysis for 657-nm ZPL (Section S11). (PDF)

AUTHOR INFORMATION

Corresponding Authors

Gabriel I. López-Morales − *Department of Physics, City University of New York, New York, New York 10031, United States*; Email: glopezmorales@gradcenter.cuny.edu

Biswanath Chakraborty − *Department of Physics, Indian Institute of Technology Jammu, Jammu 181221, India*; orcid.org/0009-0007-3679-3603; Email: biswanath.chakraborty@iitjammu.ac.in

Authors

Sakal Singla − *Department of Physics, Indian Institute of Technology Jammu, Jammu 181221, India*

Pragya Joshi − *Department of Physics, Indian Institute of Technology Jammu, Jammu 181221, India*

Suman Sarkar − *Central Instrumental Facility, Indian Institute of Technology Jammu, Jammu 181221, India*

Suman Sarkar − *Department of Materials Engineering, Indian Institute of Technology Jammu, Jammu 181221, India*

Johannes Flick − *Department of Physics, The Graduate Center, City University of New York, New York, New York 10016, United States; Center for Computational Quantum Physics, Flatiron Institute, New York, New York 10010, United States;* orcid.org/0000-0003-0273-7797

Complete contact information is available at: https://pubs.acs.org/10.1021/acs.nanolett.4c01477

Author Contributions

#S. Singla and P.J. contributed equally to this work. S. Singla, P.J., and B.C. conceived the experiments. S. Singla and P.J. did the measurements. S. Singla, P.J., B.C., and both S. Sarkar did the analysis of the experimental results. G.I.L.M. and J.F. performed the *ab-initio* calculations and related analysis. All the authors discussed the results and contributed to the manuscript.

Notes

The authors declare no competing financial interest.

ACKNOWLEDGMENTS

We thank Prof. Vinod M. Menon for helpful discussions. S. Singla and P.J. acknowledge institute fellowship from the IIT Jammu. B.C. acknowledges funding from SERB under the project grant SRG/2020/000563 and Central Instrumentation Facility at the IIT Jammu. G.I.L.M. acknowledges funding from the NSF-CREST Postdoctoral Research Fellowship (PRF) grant NSF-2208863. J.F. acknowledges funding from grant number EES-2112550 (NSF Phase II CREST Center IDEALS). The Flatiron Institute is a division of the Simon's Foundation.

REFERENCES

(1) Bourrellier, R.; Meuret, S.; Tararan, A.; Stéphan, O.; Kociak, M.; Tizei, L. H.; Zobelli, A. Bright UV single photon emission at point defects in h-BN. *Nano Lett.* **2016**, *16* (7), 4317−4321.

(2) Hayee, F.; Yu, L.; Zhang, J. L.; Ciccarino, C. J.; Nguyen, M.; Marshall, A. F.; Aharonovich, I.; Vučković, J.; Narang, P.; Heinz, T. F.; Dionne, J. A. Revealing multiple classes of stable quantum emitters in hexagonal boron nitride with correlated optical and electron microscopy. *Nature materials* **2020**, *19* (5), 534−539.

(3) Tran, T. T.; Elbadawi, C.; Totonjian, D.; Lobo, C. J.; Grosso, G.; Moon, H.; Englund, D. R.; Ford, M. J.; Aharonovich, I.; Toth, M. Robust multicolor single photon emission from point defects in hexagonal boron nitride. *ACS nano* **2016**, *10* (8), 7331−7338.

(4) Gottscholl, A.; Kianinia, M.; Soltamov, V.; Orlinskii, S.; Mamin, G.; Bradac, C.; Kasper, C.; Krambrock, K.; Sperlich, A.; Toth, M.; Aharonovich, I. Initialization and read-out of intrinsic spin defects in a van der Waals crystal at room temperature. *Nature materials* **2020**, *19* (5), 540−545.

(5) Camphausen, R.; Marini, L.; Tawfik, S. A.; Tran, T. T.; Ford, M. J.; Palomba, S. Observation of near-infrared sub-Poissonian photon emission in hexagonal boron nitride at room temperature. *APL Photonics* **2020**, *5* (7), 076103.

(6) Tran, T. T.; Bray, K.; Ford, M. J.; Toth, M.; Aharonovich, I. Quantum emission from hexagonal boron nitride monolayers. *Nature nanotechnology* **2016**, *11* (1), 37−41.

(7) Martínez, L. J.; Pelini, T.; Waselowski, V.; Maze, J. R.; Gil, B.; Cassabois, G.; Jacques, V. Efficient single photon emission from a high-purity hexagonal boron nitride crystal. *Physical review B* **2016**, *94* (12), No. 121405.

(8) Dietrich, A.; Doherty, M. W.; Aharonovich, I.; Kubanek, A. Solid-state single photon source with Fourier transform limited lines at room temperature. *Physical Review B* **2020**, *101* (8), No. 081401.

(9) Kianinia, M.; Regan, B.; Tawfik, S. A.; Tran, T. T.; Ford, M. J.; Aharonovich, I; Toth, M. Robust solid-state quantum system operating at 800 K. *Acs Photonics* **2017**, *4* (4), 768−773.

(10) Vogl, T.; Lecamwasam, R.; Buchler, B. C.; Lu, Y.; Lam, P. K. Compact cavity-enhanced single-photon generation with hexagonal boron nitride. *Acs Photonics* **2019**, *6* (8), 1955−1962.

(11) Proscia, N. V.; Jayakumar, H.; Ge, X.; Lopez-Morales, G.; Shotan, Z.; Zhou, W.; Meriles, C. A.; Menon, V. M. Microcavity-coupled emitters in hexagonal boron nitride. *Nanophotonics* **2020**, *9* (9), 2937−2944.

(12) Xu, X.; Martin, Z. O.; Sychev, D.; Lagutchev, A. S.; Chen, Y. P.; Taniguchi, T.; Watanabe, K.; Shalaev, V. M.; Boltasseva, A. Creating quantum emitters in hexagonal boron nitride deterministically on chip-compatible substrates. *Nano Letters* **2021**, *21* (19), 8182−8189.

(13) Hou, S.; Birowosuto, M. D.; Umar, S.; Anicet, M. A.; Tay, R. Y.; Coquet, P.; Tay, B. K.; Wang, H.; Teo, E. H. T. Localized emission from laser-irradiated defects in 2D hexagonal boron nitride.*2D. Materials* **2018**, *5* (1), No. 015010.

(14) Gale, A.; Li, C.; Chen, Y.; Watanabe, K.; Taniguchi, T.; Aharonovich, I.; Toth, M. Site-specific fabrication of blue quantum emitters in hexagonal boron nitride. *ACS Photonics* **2022**, *9* (6), 2170−2177.

(15) Grosso, G.; Moon, H.; Lienhard, B.; Ali, S.; Efetov, D. K.; Furchi, M. M.; Jarillo-Herrero, P.; Ford, M. J.; Aharonovich, I.; Englund, D. Tunable and high-purity room temperature single-photon emission from atomic defects in hexagonal boron nitride. *Nature communications* **2017**, *8* (1), 705.

(16) Proscia, N. V.; Shotan, Z.; Jayakumar, H.; Reddy, P.; Cohen, C.; Dollar, M.; Alkauskas, A.; Doherty, M.; Meriles, C. A.; Menon, V. M. Near-deterministic activation of room-temperature quantum emitters in hexagonal boron nitride. *Optica* **2018**, *5* (9), 1128−1134.

(17) Hernández-Mínguez, A.; Lähnemann, J.; Nakhaie, S.; Lopes, J. M. J.; Santos, P. V. Luminescent defects in a few-layer h-BN film grown by molecular beam epitaxy. *Physical Review Applied* **2018**, *10* (4), No. 044031.

(18) Mendelson, N.; Chugh, D.; Reimers, J. R.; Cheng, T. S.; Gottscholl, A.; Long, H.; Mellor, C. J.; Zettl, A.; Dyakonov, V.; Beton, P. H.; Novikov, S. V. Identifying carbon as the source of visible single-photon emission from hexagonal boron nitride. *Nature materials* **2021**, *20* (3), 321−328.

(19) Abidi, I. H.; Mendelson, N.; Tran, T. T.; Tyagi, A.; Zhuang, M.; Weng, L. T.; Özyilmaz, B.; Aharonovich, I.; Toth, M.; Luo, Z. Selective defect formation in hexagonal boron nitride.*Advanced. Optical Materials* **2019**, *7* (13), 1900397.
(20) Liu, H.; Mendelson, N.; Abidi, I. H.; Li, S.; Liu, Z.; Cai, Y.; Zhang, K.; You, J.; Tamtaji, M.; Wong, H.; Ding, Y. Rational control on quantum emitter formation in carbon-doped monolayer hexagonal boron nitride. *ACS Applied Materials & Interfaces* **2022**, *14* (2), 3189−3198.
(21) Kumar, A.; Cholsuk, C.; Zand, A.; Mishuk, M. N.; Matthes, T.; Eilenberger, F.; Suwanna, S.; Vogl, T. Localized creation of yellow single photon emitting carbon complexes in hexagonal boron nitride. *APL Materials* **2023**, *11* (7), 071108.
(22) Kumar, A.; Samaner, C.; Cholsuk, C.; Matthes, T.; Paçal, S.; Oyun, Y.; Zand, A.; Chapman, R. J.; Saerens, G.; Grange, R.; Suwanna, S. Polarization dynamics of solid-state quantum emitters. *ACS nano* **2024**, *18* (7), 5270−5281.
(23) Freysoldt, C.; Grabowski, B.; Hickel, T.; Neugebauer, J.; Kresse, G.; Janotti, A.; Van de Walle, C. G. First-principles calculations for point defects in solids. *Reviews of modern physics* **2014**, *86* (1), 253.
(24) Wickramaratne, D.; Dreyer, C. E.; Monserrat, B.; Shen, J. X.; Lyons, J. L.; Alkauskas, A.; Van de Walle, C. G. Defect identification based on first-principles calculations for deep level transient spectroscopy. *Appl. Phys. Lett.* **2018**, *113* (19), 192106.
(25) Dreyer, C. E.; Alkauskas, A.; Lyons, J. L.; Janotti, A.; Van de Walle, C. G. First-principles calculations of point defects for quantum technologies. *Annual Review of Materials Research* **2018**, *48*, 1−26.
(26) López-Morales, G. I.; Proscia, N. V.; López, G. E.; Meriles, C. A.; Menon, V. M. Toward the identification of atomic defects in hexagonal boron nitride: X-ray photoelectron spectroscopy and first-principles calculations. *arXiv Preprint* **2018**, DOI: 10.48550/arXiv.1811.05924.
(27) Weston, L.; Wickramaratne, D.; Mackoit, M.; Alkauskas, A.; Van de Walle, C. G. Native point defects and impurities in hexagonal boron nitride. *Physical Review B* **2018**, *97*, No. 214104.
(28) Tawfik, S. A.; Ali, S.; Fronzi, M.; Kianinia, M.; Tran, T. T.; Stampfl, C.; Aharonovich, I.; Toth, M.; Ford, M. J. First-principles investigation of quantum emission from hBN defects. *Nanoscale* **2017**, *9* (36), 13575−13582.
(29) Li, S.; Gali, A. Identification of an oxygen defect in hexagonal boron nitride. *The Journal of Physical Chemistry Letters* **2022**, *13* (41), 9544−9551.
(30) Gao, S.; Chen, H. Y.; Bernardi, M. Radiative properties of quantum emitters in boron nitride from excited state calculations and Bayesian analysis. *npj Computational Materials* **2021**, *7* (1), 85.
(31) Auburger, P.; Gali, A. Towards ab initio identification of paramagnetic substitutional carbon defects in hexagonal boron nitride acting as quantum bits. *Physical Review B* **2021**, *104* (7), No. 075410.
(32) Winter, M.; Bousquet, M. H. E.; Jacquemin, D.; Duchemin, I.; Blase, X. Photoluminescent properties of the carbon-dimer defect in hexagonal boron-nitride: A many-body finite-size cluster approach. *Phys. Rev. Mater.* **2021**, *5* (9), No. 095201.
(33) Mackoit-Sinkevičienė, M.; Maciaszek, M.; Van de Walle, C. G.; Alkauskas, A. Carbon dimer defect as a source of the 4.1 eV luminescence in hexagonal boron nitride. *Appl. Phys. Lett.* **2019**, *115* (21), 212101.
(34) Jara, C.; Rauch, T.; Botti, S.; Marques, M. A.; Norambuena, A.; Coto, R.; Castellanos-Águila, J. E.; Maze, J. R.; Munoz, F. First-principles identification of single photon emitters based on carbon clusters in hexagonal boron nitride.*The. Journal of Physical Chemistry A* **2021**, *125* (6), 1325−1335.
(35) Turiansky, M. E.; Alkauskas, A.; Bassett, L. C.; Van de Walle, C. G. Dangling bonds in hexagonal boron nitride as single-photon emitters. *Physical review letters* **2019**, *123* (12), No. 127401.
(36) Reich, S.; Ferrari, A. C.; Arenal, R.; Loiseau, A.; Bello, I.; Robertson, J. Resonant Raman scattering in cubic and hexagonal boron nitride. *Physical Review B* **2005**, *71* (20), No. 205201.
(37) Li, S. X.; Ichihara, T.; Park, H.; He, G.; Kozawa, D.; Wen, Y.; Koman, V. B.; Zeng, Y.; Kuehne, M.; Yuan, Z.; Faucher, S. Prolonged photostability in hexagonal boron nitride quantum emitters. *Communications Materials* **2023**, *4* (1), 19.
(38) Krivanek, O. L.; Chisholm, M. F.; Nicolosi, V.; Pennycook, T. J.; Corbin, G. J.; Dellby, N.; Murfitt, M. F.; Own, C. S.; Szilagyi, Z. S.; Oxley, M. P.; Pantelides, S. T. Atom-by-atom structural and chemical analysis by annular dark-field electron microscopy. *Nature* **2010**, *464* (7288), 571−574.
(39) Park, H.; Wen, Y.; Li, S. X.; Choi, W.; Lee, G. D.; Strano, M.; Warner, J. H. Atomically precise control of carbon insertion into hBN monolayer point vacancies using a focused electron beam guide. *Small* **2021**, *17* (23), 2100693.
(40) Wang, S.; March, K.; Ponce, F. A.; Rez, P. Identification of point defects using high-resolution electron energy loss spectroscopy. *Physical Review B* **2019**, *99* (11), No. 115312.
(41) Suenaga, K.; Koshino, M. Atom-by-atom spectroscopy at graphene edge. *Nature* **2010**, *468* (7327), 1088−1090.
(42) Warner, J. H.; Lin, Y. C.; He, K.; Koshino, M.; Suenaga, K. Stability and spectroscopy of single nitrogen dopants in graphene at elevated temperatures. *ACS nano* **2014**, *8* (11), 11806−11815.
(43) Cretu, O.; Lin, Y. C.; Koshino, M.; Tizei, L. H.; Liu, Z.; Suenaga, K. Structure and local chemical properties of boron-terminated tetravacancies in hexagonal boron nitride. *Phys. Rev. Lett.* **2015**, *114* (7), No. 075502.
(44) Suenaga, K.; Kobayashi, H.; Koshino, M. Core-level spectroscopy of point defects in single layer h-BN. *Physical review letters* **2012**, *108* (7), No. 075501.
(45) Fournier, C.; Plaud, A.; Roux, S.; Pierret, A.; Rosticher, M.; Watanabe, K.; Taniguchi, T.; Buil, S.; Quélin, X.; Barjon, J.; Hermier, J. P. Position-controlled quantum emitters with reproducible emission wavelength in hexagonal boron nitride. *Nature communications* **2021**, *12* (1), 3779.
(46) Bhunia, A.; Joshi, P.; Singh, N.; Chakraborty, B.; Nair, R. V. Site-specific stable deterministic single photon emitters with low Huang-Rhys value in layered hexagonal boron nitride at room temperature. *arXiv Preprint* **2023**, DOI: 10.48550/arXiv.2307.11433.
(47) Aharonovich, I.; Tetienne, J. P.; Toth, M. Quantum emitters in hexagonal boron nitride. *Nano Letters* **2022**, *22* (23), 9227−9235.
(48) Zhong, D.; Gao, S.; Saccone, M.; Greer, J. R.; Bernardi, M.; Nadj-Perge, S.; Faraon, A. Carbon-Related Quantum Emitter in Hexagonal Boron Nitride with Homogeneous Energy and 3-Fold Polarization. Nano Letters. *Nano Letters* **2024**, *24* (4), 1106−1113.
(49) Qiu, Z.; Vaklinova, K.; Huang, P.; Grzeszczyk, M.; Yang, H.; Watanabe, K.; Taniguchi, T.; Novoselov, K. S.; Lu, J.; Koperski, M. Atomic structure of carbon centres in hBN: towards engineering of single photon sources. *arXiv Preprint* **2021**, DOI: 10.48550/arXiv.2110.07842.
(50) Tan, Q.; Lai, J. M.; Liu, X. L.; Guo, D.; Xue, Y.; Dou, X.; Sun, B. Q.; Deng, H. X.; Tan, P. H.; Aharonovich, I.; Gao, W. Donor−acceptor pair quantum emitters in hexagonal boron nitride. *Nano Letters* **2022**, *22* (3), 1331−1337.
(51) Maciaszek, M.; Razinkovas, L.; Alkauskas, A. Thermodynamics of carbon point defects in hexagonal boron nitride. *Physical Review Materials* **2022**, *6* (1), No. 014005.
(52) Marye, S. A.; Kumar, R. R.; Useinov, A.; Tumilty, N. Thermal stability, work function and Fermi level analysis of 2D multi-layered hexagonal boron nitride films. *Microelectron. Eng.* **2024**, *283*, No. 112106.
(53) Benedek, Z.; Babar, R.; Ganyecz, Á.; Szilvási, T.; Legeza, Ö.; Barcza, G.; Ivády, V. Symmetric carbon tetramers forming spin qubits in hexagonal boron nitride. *npj Computational Materials* **2023**, *9* (1), 187.
(54) Kresse, G.; Furthmüller, J. Efficient iterative schemes for ab initio total-energy calculations using a plane-wave basis set. *Physical review B* **1996**, *54* (16), 11169.
(55) Kresse, G.; Joubert, D. From ultrasoft pseudopotentials to the projector augmented-wave method. *Physical review b* **1999**, *59* (3), No. 1758.

https://doi.org/10.1021/acs.nanolett.4c01477
Nano Lett. 2024, 24, 9212−9220

(56) Perdew, J. P.; Burke, K.; Ernzerhof, M. Generalized gradient approximation made simple. *Physical review letters* **1996**, *77* (18), No. 3865.
(57) Heyd, J.; Scuseria, G. E.; Ernzerhof, M. Hybrid functionals based on a screened Coulomb potential. *The Journal of chemical physics* **2003**, *118* (18), 8207−8215.
(58) Grimme, S.; Antony, J.; Ehrlich, S.; Krieg, H. A consistent and accurate ab initio parametrization of density functional dispersion correction (DFT-D) for the 94 elements H-Pu. *The Journal of chemical physics* **2010**, *132* (15), 154104.
(59) Grimme, S.; Ehrlich, S.; Goerigk, L. Effect of the damping function in dispersion corrected density functional theory. *Journal of computational chemistry* **2011**, *32* (7), 1456−1465.
(60) Smith, D. G.; Burns, L. A.; Patkowski, K.; Sherrill, C. D. Revised damping parameters for the D3 dispersion correction to density functional theory. *The journal of physical chemistry letters* **2016**, *7* (12), 2197−2203.

https://doi.org/10.1021/acs.nanolett.4c01477
Nano Lett. 2024, 24, 9212−9220